Neuroscience 358 (2017) 227–237

NADPH OXIDASE CONTRIBUTES TO STREPTOZOTOCIN-INDUCED NEURODEGENERATION

KATHERINE GARCIA RAVELLI, [a] **BARBARA DOS ANJOS ROSÁRIO,** [a] **ANDREA RODRIGUES VASCONCELOS,** [b] **CRISTOFORO SCAVONE,** [b] **ROSANA CAMARINI,** [b] **MARINA S. HERNANDES** [c]* **AND LUIZ ROBERTO BRITTO** [a]

[a] *Department of Physiology and Biophysics, University of São Paulo, São Paulo, Brazil*

[b] *Department of Pharmacology, University of São Paulo, São Paulo, Brazil*

[c] *Division of Cardiology, Department of Medicine, Emory University, Atlanta, GA, United States*

Abstract—Alzheimer's disease (AD) is a neurodegenerative disorder characterized by the progressive loss of memory. The neurodegeneration induced by AD has been linked to oxidative damage. However, little is known about the involvement of NADPH oxidase 2 (Nox2), a multisubunit enzyme that catalyzes the reduction of oxygen to produce reactive oxygen species, in the pathogenesis of AD. The main purpose of this study was to investigate the involvement of Nox2 in memory, in AD-related brain abnormalities, oxidative damage, inflammation and neuronal death in the hippocampus in the streptozotocin (STZ)-induced AD-like state by comparing the effects of that drug on mice lacking gp91$^{phox-/-}$ and wild-type (Wt) mice. Nox2 gene expression was found increased in Wt mice after STZ injection. In object recognition test, Wt mice injected with STZ presented impairment in short- and long-term memory, which was not observed following Nox2 deletion. STZ treatment induced increased phosphorylation of Tau and increased amyloid-β, apoptosis-inducing factor (AIF) and astrocyte and microglial markers expression in Wt mice but not in gp91$^{phox-/-}$. STZ treatment increased oxidative damage and pro-inflammatory cytokines' release in Wt mice, which was not observed in gp91$^{phox-/-}$ mice. Nox2 deletion had a positive effect on the IL-10 baseline production, suggesting that this cytokine might contribute to the neuroprotection mechanism against STZ-induced neurodegeneration. In summary, our data suggest that the Nox2-dependent reactive oxygen species (ROS) generation contributes to the STZ-induced AD-like state.

Keywords: Alzheimer's disease, streptozotocin, Nox2, cytokines.

INTRODUCTION

Alzheimer's disease (AD) is a degenerative disorder that usually begins with a subtle memory loss that slowly becomes more severe and, eventually, incapacitating. Other common clinical symptoms of AD include: confusion, poor judgment, language disturbance, agitation and hallucinations (Bird, 2008). In advanced stages of the disease, the deceleration of motor functions leads to a condition similar to parkinsonism (Selkoe, 2001). Several abnormalities were observed in the brain glucose metabolism of patients with sporadic AD. Both the impairment of neuronal insulin signaling and the impairment in the function of translation of insulin receptors have been associated with AD development (Moloney et al., 2010; Liu et al., 2011a,b; Bomfim et al., 2012; Talbot et al., 2012; Yarchoan et al., 2014).

The neuropathological changes of AD brain mainly affect neocortex, hippocampus, entorhinal cortex and some subcortical areas (Spires and Hyman, 2005) and include: the accumulation of amyloid plaques (composed primarily by β-amyloid peptide (Aβ)) (Hardy and Allsop, 1991) and the accumulation of neurofibrillary tangles, neuropil threads and dystrophic neurites containing hyperphosphorylated Tau protein. These changes are accompanied by astrocyte and microglial cell activation (Serrano-Pozo et al., 2011). When chronically activated, microglia generates reactive oxygen (ROS) and nitrogen (RNS) species (Wilkinson et al., 2012), in addition to cytokines, interleukins (IL) and other cytotoxic molecules (Heneka et al., 2015). The activation of microglial cells leads to NADPH oxidase (Nox)-dependent ROS production in the hippocampus resulting in significant neuronal death (Park et al., 2009; Bonda et al., 2010).

The intracerebroventricular (icv) injections of streptozotocin (STZ), a compound synthesized by *Streptomycetes achromogenes* (Szkudelski, 2001) have been used to induce AD-like state in rodents. STZ icv injections induce a progressive deterioration of cognitive function in parallel to changes in glucose and energy metabolism, oxidative stress (Grunblatt et al., 2004), accumulation of Aβ (Knezovic et al., 2015; Ravelli et al., 2017) and increased Tau phosphorylation (Chen et al., 2013; Ravelli et al., 2017). The most prominent brain abnormality in this model is neuroinflammation, reflected

*Corresponding author. Address: Department of Medicine, Division of Cardiology, Emory University, 101 Woodruff Circle, 3331 WMB, Atlanta, GA 30322, United States.
E-mail address: mshern2@emory.edu (M. S. Hernandes).

Abbreviations: 3-NT, 3-nitrotyrosine; 4-HNE, 4-hydroxy-2 nonenal; AD, Alzheimer's disease; Aβ, β-amyloid peptide; AIF, apoptosis-inducing factor; IL, interleukins; Nox, NADPH oxidase; RNS, reactive nitrogen species; ROS, reactive oxygen species; STZ, streptozotocin; Wt, wild type.

http://dx.doi.org/10.1016/j.neuroscience.2017.06.050
0306-4522/

by astrogliosis and microglial activation (Chen et al., 2013).

NADPH oxidases are a family of enzymes dedicated to the production of ROS. These enzymes are able to catalyze the production of superoxide anion by reducing an electron of molecular oxygen, using NADPH as an electron donor. The prototypical Nox, known as Nox2, is composed of three subunits ($p40^{PHOX}$, $p47^{PHOX}$ and $p67^{PHOX}$) present in the cytosol as a complex and two membrane subunits ($gp91^{phox}$ and $p22^{phox}$) composing the cytochrome b558. After a stimulus, the activation of a low-molecular weight G protein (Rac1 or Rac2) and phosphorylation of $p47^{phox}$ initiate migration of the cytosolic complex to the plasma membrane (Hernandes and Britto, 2012), where it associates with cytochrome b_{558} forming a functional Nox complex capable of reducing oxygen to superoxide (Hernandes et al., 2013).

Nox-derived ROS seem to mediate cerebrovascular dysfunctions induced by Aβ (Block, 2008). *In vitro* experiments demonstrated that Nox inhibition by apocynin, a nonspecific pharmacological Nox2 inhibitor, decreased the ability of the β-amyloid peptide to induce degeneration and to trigger morphological changes in neurons (Bruce-Keller et al., 2010). However, in a transgenic model of AD, apocynin treatment did not improve behavioral or neuropathological deficits despite causing a reduction in oxidative stress in the cerebral cortex (Dumont et al., 2011). Gp91ds-tat, a Nox2 peptide inhibitor, was able to decrease the generation of ROS induced by exogenous Aβ in the somatosensory cortex of mice. Moreover, exogenous Aβ was not able to trigger the production of ROS in mice lacking the catalytic subunit of Nox2 ($gp91^{phox}$). Furthermore, no evidence of oxidative stress was observed in transgenic mice overexpressing the amyloid precursor protein but lacking $gp91^{phox}$ (Park et al., 2005).

Nox2-derived ROS has emerged as an important mechanism in the pathogenesis of AD. However, there has been no study directly testing the involvement of Nox2 in cognitive impairment induced by STZ, nor has its role in Tau phosphorylation, oxidative damage, neuronal death and neuroinflammation induced by STZ been investigated. In light of those facts, the main purpose of this study was to investigate the involvement of Nox2 in short- and long-term memory, in AD-related brain abnormalities, inflammation and neuronal death in the hippocampus in the STZ-induced AD-like state by comparing the effects of that drug on mice lacking $gp91^{phox-/-}$ and wild-type mice (Wt) (C57BL/6).

EXPERIMENTAL PROCEDURES

Animals

Male $gp91^{Phox-/-}$ mice (25–30 g) were purchased from the Jackson Laboratory (Bar Harbor, Maine, USA) and maintained on a C57BL/6 background. The animals were maintained on a 12: 12 h light–dark cycle and with free access to food and water. All animal protocols were approved by the Institutional Animal Care and Use Committee of the Institute of Biomedical Sciences of the University of Sao Paulo, Brazil (protocol number: 098/2012).

Surgical procedures

Surgical procedures were performed as previously described (Ravelli et al., 2017). Mice were anesthetized initially with 5% isoflurane for induction and then maintained with 2–3% isoflurane throughout the duration of surgery. STZ (Sigma, St. Louis, MO) was dissolved in citrate buffer (0.05 mol/L, pH 4.5) immediately before injection. Mice were placed in a stereotaxic apparatus (Insight Ltda, SP, Brazil) and the STZ group was injected bilaterally in the lateral ventricles with STZ (3 mg/kg) in two divided doses (1.5 mg/kg each), on days 1 and 3. The concentration was adjusted so as to deliver 1.5 μl per injection. Control mice were injected with citrate buffer. The bregma coordinates used for injection were: AP: −0.5 mm; ML: ±1.1 mm; DV: −2.8 mm. The injections were performed using a Hamilton syringe (model 701) and conducted at a rate of 0.5 μL/min. The needle was left *in situ* for 3 min to prevent back flow. Clinical signs were monitored daily after the surgery, including general body condition and dehydration. The mice were euthanized for analysis 14 days after the surgery (Ravelli et al., 2017).

Real-time PCR

Tissue from the hippocampi from Wt mice ($n = 6$ for each group) were directly homogenized in 1 ml TRIzol (Invitrogen, Carlsbad, CA, USA) and total RNA was isolated following the manufacturer's suggested protocol. Following two chloroform extraction steps, RNA was precipitated with isopropanol and the pellet washed twice in 70% ethanol. Samples were resuspended in DEPC-treated water and RNA was quantified by measuring the optical density at 260 nm using a Nanodrop-1000 spectrophotometer. One microgram total RNA was reverse transcribed using the Promega Reverse Transcription System (Madison, WI, USA). Total RNA was incubated at 70 °C for 10 min. The solution was mixed with 4 μL of $MgCl_2$ (25 mM), 2 μL of 5 × RT buffer, 2 μL of dNTP mixture (10 mM), 0.5 μl of RNAsin inhibitor (40U/μl), 0.5 μl of AMV reverse transcriptase, and 1 μL of oligodT primer (0.5 μg). The reactions were incubated at 16 °C for 30 min, 42 °C for 30 min, 85 °C for 5 min and then kept at 4 °C. qPCR was carried out with SYBR Green Real-Time Selected Master Mix (Applied Biosystems, CA, USA) according to the user guide. The reaction volume was 20 μL with 2 μL diluted cDNA, 10 μL of SYBR Master Mix, and 500 nM of each primer. Amplification and PCR product detection were performed with the ABI prism 7500 real time-PCR System (Applied Biosystems, USA). The conditions for PCR were as follows: 50 °C for 2 min, 95 °C for 2 min, then 30 cycles of 95 °C for 15 s, 60 °C for 1 min, and 72 °C for 15 s. The specificity of the SYBR® green assay was confirmed by melting-point analysis. Expression data were calculated from the cycle threshold (Ct) value using the ΔCt method for quantification (Dussault and Pouliot, 2006). Gene expression of GAPDH was used for normal-

ization. Results were expressed as percent increases. Sequences used were: Nox2 (sense 5′-TCAAGACCATTG CAAGTGAACAC-3′; antisense 5′-TCAGGGCCACACAG GAAAA-3′) and GAPDH (sense 5′-GTGCAGTGC CAGCCTCGTCC-3′; antisense 5′-CAGGCGCCCAAT ACGGCCAA -3′).

Object recognition test

The behavioral assay occurred in three different phases: a habituation phase, a sample phase, and a test phase. In the first day (habituation phase), mice ($n = 5$ injected with citrate and 8 injected with STZ) were habituated to the open-field apparatus ($35 \times 29 \times 16$ cm) for 10 min and then were taken back to their home cages. This procedure was repeated 3 times, with 30-min intervals. On the second day (sample phase), two identical objects (A and B) were placed at fixed distances in a symmetric position from the center of arena. The animals were placed in the arena facing the wall opposite to the objects and were allowed to explore the objects and the arena for 10 min. One and 24 h later, during the testing phase, one of the original objects (A) was replaced with a novel object of different shape (C and D, respectively) and mice were allowed to explore novel objects for 5 min.

The total exploration (sniffing, licking or touching the object with the nose or with the forelimbs or directing the nose at a distance $\leq$1 cm to the object) time of the objects during the first 5 min was quantified in the sample and test phases (1 and 24 h). Data collection was performed using a video tracking system Pinnacle Studio (Pinnacle Systems, Mountain View, CA, USA). After each session, the arena and objects were cleaned with 5% ethanol to ensure that behavior of animals was not guided by odor cues.

Calculation of the interest in a new object in the testing phase, which is called the Investigation Ratio (IR), was calculated as the ratio between the time spent by exploration of a new object (T_{new}) to the total time spent by exploration of both objects (T_{total}) ($IR = T_{new}/T_{total}$).

Immunoblotting

Animals ($n = 3$ injected with citrate and 5 injected with STZ) were sacrificed by decapitation and the hippocampi were quickly collected and homogenized in extraction buffer (Tris, pH 7.4, 100 mM; sodium pyrophosphate 100 mM; sodium fluoride 100 mM; EDTA 10 mM, sodium orthovanadate 10 mM; PMSF 2 mM; aprotinin 0.01 mg/ml). The homogenates were subjected to centrifugation for 15 min at 12,000 rpm at 4 °C and the protein concentration of the supernatant was determined using the Bradford method (Bio-Rad, CA, USA). The samples were stored in sample buffer (Tris/HCl 500 mM, pH 6.8; 10% of SDS, 0.25% of bromophenol Blue; 10% of 2-mercaptoethanol and 50% glycerol) at −70 °C until use.

The samples from the homogenate (30 μg of protein) were run on an acrylamide gel and electrotransferred to nitrocellulose membranes (Millipore, Billerica, MA, USA) at 100 V for 80 min using a Trans-Blot cell. The nitrocellulose membranes were then blocked for 2 h at room temperature and incubated overnight at 4 °C with following antibodies: monoclonal anti-rabbit amyloid β (1:1000; Santa Cruz Biotechnology, USA), monoclonal anti-mouse Tau (1:2000; Sigma Chemical Co., USA), monoclonal anti-rabbit Phosphorylated Tau ($Ser^{199/202}$) (1:2000; Sigma Chemical Co., USA), monoclonal anti-rabbit GFAP (1:1000; Santa Cruz Biotechnology, USA), monoclonal anti-mouse Ox-42 (1:1000; Invitrogen, USA), polyclonal anti-goat apoptosis-inducing factor (AIF, 1:500; Santa Cruz Biotechnology, TX, USA), polyclonal anti-rabbit 4-Hydroxy-2 nonenal (4-HNE, 1:500; Alpha Diagnostic, TX, USA), monoclonal-anti-mouse 3-nitrotyrosine (3-NT, 1:500; Santa Cruz Biotechnology, USA) and monoclonal anti-mouse β-actin (1:5000; Sigma Chemical Co., USA). After incubation with the appropriate HRP-conjugated secondary antibodies, the immune reaction was developed by enhanced chemiluminescence (ECL) reagent (Bio-Rad, CA, USA) according to the manufacturer's instructions. The target proteins were detected using a C-DiGit Western blot scanner (LI-COR, USA). β-actin was used as an internal control. The quantification of band intensity was performed with ImageJ (National Institutes of Health, USA).

Immunohistochemistry

Mice ($n = 3$ injected with citrate and 5 injected with STZ) were deeply anesthetized with ketamine hydrochloride (100 mg/kg of body weight, i.m.) and xylazine (16 mg/kg of body weight, i.m.) and transcardially perfused with a buffered 0.9% saline solution, followed by a fixative solution consisting of 4% paraformaldehyde (PFA) dissolved in 0.1 M phosphate buffer (PB, pH 7.4). The brains were collected and after 4 h post-fixation in PFA solution they were transferred to a 30% sucrose PB solution, to ensure cryoprotection and stored at 4 °C during at least 48 h. Coronal sections (30 μm) were obtained on a sliding microtome and were incubated overnight with anti-OX42 (CD11b/c, Biosciences, CA, USA) and anti-GFAP (Immunon, Pittsburgh, PA, USA), diluted 1 : 1000 in 0.3% of Triton X-100, containing 0.05% normal donkey serum. Following 3 washes with PB, sections were incubated for 2 h with a biotinylated secondary antibody, then with the avidin–biotin complex (1 : 100; ABC Elite kit, Vector Labs, Burlingame, CA, USA). The sections reacted with 0.05% 3,3-diaminobenzidine and 0.01% hydrogen peroxide in PB. Intensification was conducted with 0.05% osmium tetroxide in water.

Images were captured using a Nikon DMX1200 digital camera and were quantified by using integrated optical density, normalized to the background optical density, measured in the same way in the same section using Image J (NIH). Immunostaining was evaluated in terms of optical density within areas of 0.04 mm^2 and 0.03 mm^2, respectively for CA1 and CA3 regions of the hippocampus. Measurements were taken from 5 different hippocampi-containing sections for each animal.

Multiplex analysis of cytokines

Concentrations of IL-4, IL-1β, IL-2, IL-10, IFN-γ, TNF-α, IL-12/23 (p40) and IL-12 (p70) were simultaneously measured in extracts from homogenized hippocampus using a mouse multiplexed bead-based immunoassay Milliplex Map Kit, MCYTOMAG-70 K (Millipore, Billerica, MA, USA) (Moncunill et al., 2013). Hippocampi of Wt and gp91$^{phox-/-}$ mice (n = 5 injected with citrate and 8 injected with STZ) were collected and homogenized in a buffer containing 150 mM NaCl, 0.05% Tween-20, 1 mM PMSF, 20 mM Tris–HCl (pH 7.5), 2.5 μg/ml antipain and 2.5 μg/ml leupeptin. The samples were centrifuged at 20,000×g for 2 min at 4 °C and the supernatant was used for the analysis. The protein concentration was measured using the Bradford method (Bio-Rad, CA, USA).

Cytokine concentrations were determined using antibodies for each analyte covalently immobilized to a set of microspheres (Fox et al., 2005). The analytes on the surface of microspheres were then detected by a cocktail of biotinylated antibodies. The reporter fluorescent signal was measured with a Luminex100 reader (Luminex Corp., Austin, TX, USA) with xPONENT 3.1 software. Standard curves for each cytokine were generated using standards included in the kit diluted in a lysis buffer for tissue samples. Cytokine concentrations in the samples were determined with a 5-parameter logistic curve and normalized to the amount of protein in each sample. Final concentrations were calculated from the mean fluorescence intensity and expressed in pg/mg. All incubation steps were performed at room temperature and in the dark.

Statistical analysis

Data were expressed as means ± standard error of the mean (SEM). For individual comparisons, statistical analysis was performed using unpaired Student's t-test. Statistical analysis for STZ-induced changes in WT and gp91$^{phox-/-}$ mice were performed by a Two-way analysis of variance (ANOVA), followed by pairwise comparisons (Tukey's HSD test). In all cases, $p \leq 0.05$ was considered to be statistically significant. Statistical analyses of data were generated using GraphPad Prism, version 3.02, and Statistica 13.

RESULTS

Effect of STZ on Nox2 mRNA expression

In order to test if Nox2 can be induced by icv STZ treatment, the Nox2 mRNA gene expression was evaluated by RT-PCR in hippocampus. Nox2 mRNA expression was found to be upregulated by 466% when compared to the control group (Fig. 1).

Nox2 mediates STZ-induced oxidative stress

The levels of 4-HNE increased 117% in Wt animals following the STZ treatment ($F(1, 12) = 5.1942$, $p = 0.04$ for treatment). The same treatment did not alter significantly the expression of 4-HNE in the hippocampus of gp91$^{phox-/-}$ mice (Fig. 2A).

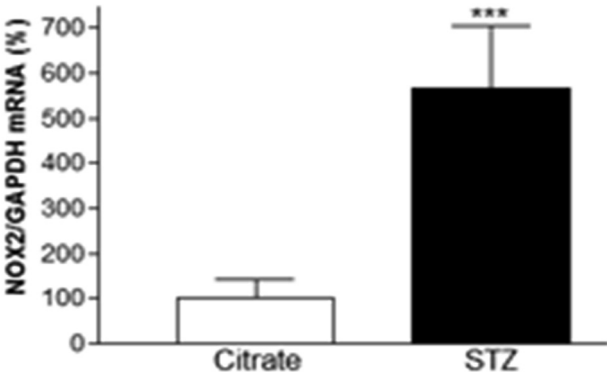

Fig. 1. Effects of STZ on Nox2 activation. Effect of STZ on mRNA of Nox2 isoform in the hippocampus of Wt mice. GAPDH was used as an internal control. (n = 6) $^{*}P < 0.05$ (Student's t-test). STZ = streptozotocin.

Similarly, the levels of 3-NT were found increased (295%) in Wt mice after STZ treatment ($F(1, 13) = 6.8093$, $p = 0.02$ for treatment), which was not observed in gp91$^{phox-/-}$ mice (Fig. 2B).

Nox2 deletion abrogates short- and long-term memory loss induced by STZ

The Novel Object Recognition Test was performed 14 days after the first STZ injection. No differences were found between Wt and gp91$^{phox-/-}$ mice in the total time of object exploration (both objects) during the different phases (not shown).

STZ-injected Wt mice spent significant less time ($F(1, 19) = 6.6720$, $p = 0.01$ for treatment and $F(1, 19) = 8.0849$, $p = 0.01$ for treatment × gene) exploring the novel object than the familiar object when compared to citrate-injected control Wt mice following a 1-h delay. No differences were found between gp91$^{phox-/-}$ STZ-treated mice and their respective control group (citrate-injected gp91$^{phox-/-}$ mice, Fig. 3 A). Similar results were obtained when memory retention was tested 24 h after the sample session ($F(1, 19) = 14.194$, $p = 0.001$ for treatment and $F(1, 19) = 7.1526$, $p = 0.01$ for treatment × gene) (Fig. 3 B).

Altogether, these results indicated that STZ treatment significantly impaired object recognition memory following 1-h or 24-h delay in Wt mice, which was not observed in gp91$^{phox-/-}$ mice.

Nox2 mediates *Tau phosphorylation and Aβ* and AIF protein expression

We found increased hippocampal Aβ protein levels (111%) in Wt animals following the STZ treatment ($F(1, 15) = 4.8211$, $p = 0.04$) for treatment and $F(1, 15) = 6.4534$, $p = 0.02$ for treatment × gene). Treatment with STZ did not alter the expression of this protein in the hippocampus of gp91$^{phox-/-}$ mice. However, the basal expression of Aβ was found significantly increased (140%) in gp91$^{phox-/-}$ mice when compared to Wt mice ($F(1, 15) = 10.264$, $p = 0.005$ for gene) (Fig. 4 A). Moreover, we observed that the treatment with STZ

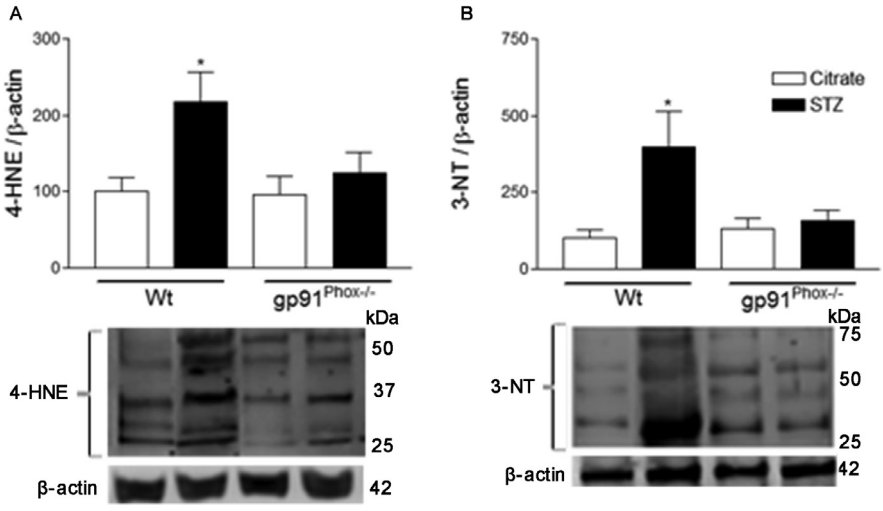

Fig. 2. Effect of STZ on hippocampal oxidative stress in Wt and gp91$^{phox-/-}$ mice. Oxidative damage was analyzed by Western blotting for the expression of 4-HNE as marker of lipid peroxidation (A) and 3-NT as marker of protein nitration. The graphs represent mean ratio of 4-HNE (n = 3–5) and 3-NT (n = 3–5) densitometric data in relation to β-actin. $^{*}P < 0.05$ *vs* Wt control group (Tukey's test). STZ = streptozotocin, 4-HNE = 4-Hydroxy-2 nonenal, 3-NT = 3-nitrotyrosine.

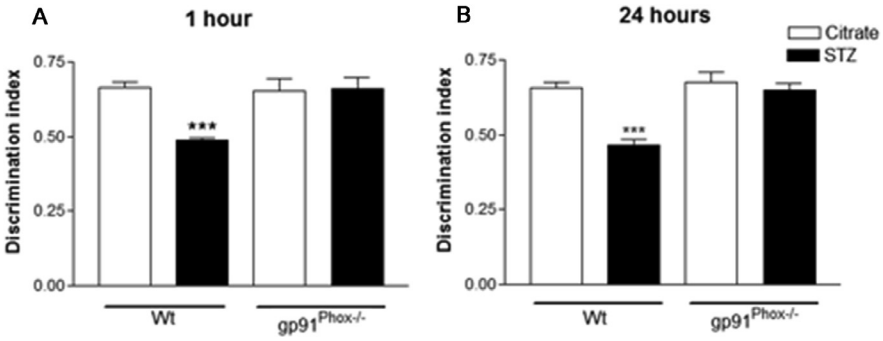

Fig. 3. Effect of STZ on short-term and long-term memory in Wt and gp91$^{phox-/-}$ mice. Memory was assessed by novel object recognition test. Object discrimination during the test phase is presented as a discrimination index (time exploring the novel object/total time for exploring). (n = 4–8) $^{***}P < 0.001$ *vs* Wt control group (Tukey's test). STZ = streptozotocin.

increased the ratio of pTau/Tau (144%) in Wt mice ($F(1, 11) = 12.490$, $p = 0.004$ for treatment and $F(1, 11) = 12.898$, $p = 0.004$ for treatment × gene), suggesting increased Tau phosphorylation. The same increase was not observed in gp91$^{phox-/-}$ mice (Fig. 4 B) following STZ injection. Furthermore, increased expression of AIF (254%) was observed in Wt animals injected with STZ when compared to citrate-injected mice ($F(1, 10) = 25.027$, $p = 0.0005$ for treatment and $F(1, 10) = 9{,}4648$, $p = 0.01$ for treatment × gene). Increased AIF expression was not observed in gp91$^{phox-/-}$ STZ-injected mice (Fig. 4 C).

Glial cells activation following the STZ treatment is mediated by Nox2

In STZ-injected Wt mice, we observed an increase in OX42 protein expression, a microglial cell marker, when compared to Wt citrate-injected mice ($F(1, 11) = 9.5539$, $p = 0.01$ for treatment and $F(1, 11) = 4.3954$, $p = 0.05$ for treatment × gene). In contrast, gp91$^{phox-/-}$ STZ-treated mice did not show increase in microglial activation when compared to gp91$^{phox-/-}$ citrate-injected mice (Fig. 5 A). Analysis of OX42 distribution throughout the hippocampus revealed an increased immunoreactivity into CA1 (166%) ($F(1, 11) = 8.0342$, $p = 0.01$ for treatment and $F(1, 11) = 4.6276$, $p = 0.05$ for treatment × gene) (Fig. 5 D) and CA3 (Fig. 5 E) areas (73%) ($F(1, 9) = 7.9093$, $p = 0.02$ for treatment and $F(1, 9) = 14.221$, $p = 0.004$ for treatment × gene) in the hippocampus of STZ-injected Wt mice.

Analysis of GFAP, an astrocyte marker, revealed an increased expression of this marker in STZ-injected Wt mice (70%) compared to control ($F(1, 9) = 7.1167$, $p = 0.02$ for treatment), which was not observed in gp91$^{phox-/-}$ mice (Fig. 5 F). Analysis of GFAP distribution revealed its increased immunoreactivity into the CA1 (81%) area of the hippocampus ($F(1, 11) = 8.2031$, $p = 0.01540$ for treatment and $F(1, 11) = 7.0730$, $p = 0.02$ for treatment × gene) (Fig. 5 I).

STZ-induced IFN-γ, IL-1β, IL-2, IL-4, IL-12/23 and IL-12 is mediated by Nox2

In Wt animals, STZ significantly increased the production of IFN-γ ($F(1, 22) = 10.757$, $p = 0.003$ for treatment and $F(1, 22) = 10.658$, $p = 0.003$ for treatment × gene), IL-1β ($F(1, 21) = 8.3331$, $p = 0.008$ for treatment and $F(1, 21) = 8.8464$, $p = 0.007$ for treatment × gene), IL-2 ($F(1, 18) = 7.9539$, $p = 0.01$ for treatment × gene), IL-4 ($F(1, 24) = 8.7116$, $p = 0.006$ for treatment and $F(1, 24) = 9.1459$, $p = 0.005$ for treatment × gene), IL-12/23 (p40) ($F(1, 18) = 6.6003$, $p = 0.01$ for treatment and $F(1, 18) = 11.141$, $p = 0.003$ for treatment × gene) and IL-12 (p70) ($F(1, 26) = 8.8610$, $p = 0.006$ for treatment × gene), which was not observed in gp91$^{phox-/-}$ mice. STZ did not induce TNF-α release in either Wt or gp91$^{phox-/-}$ mice. The baseline protein concentration of IL-10 was found significantly increased in gp91$^{phox-/-}$ mice ($F(1, 24) = 18.339$, $p = 0.0002$ for gene), when compared to Wt mice (Fig. 6).

DISCUSSION

In this study, we investigated the involvement of Nox2 in short- and long-term memory impairment, oxidative

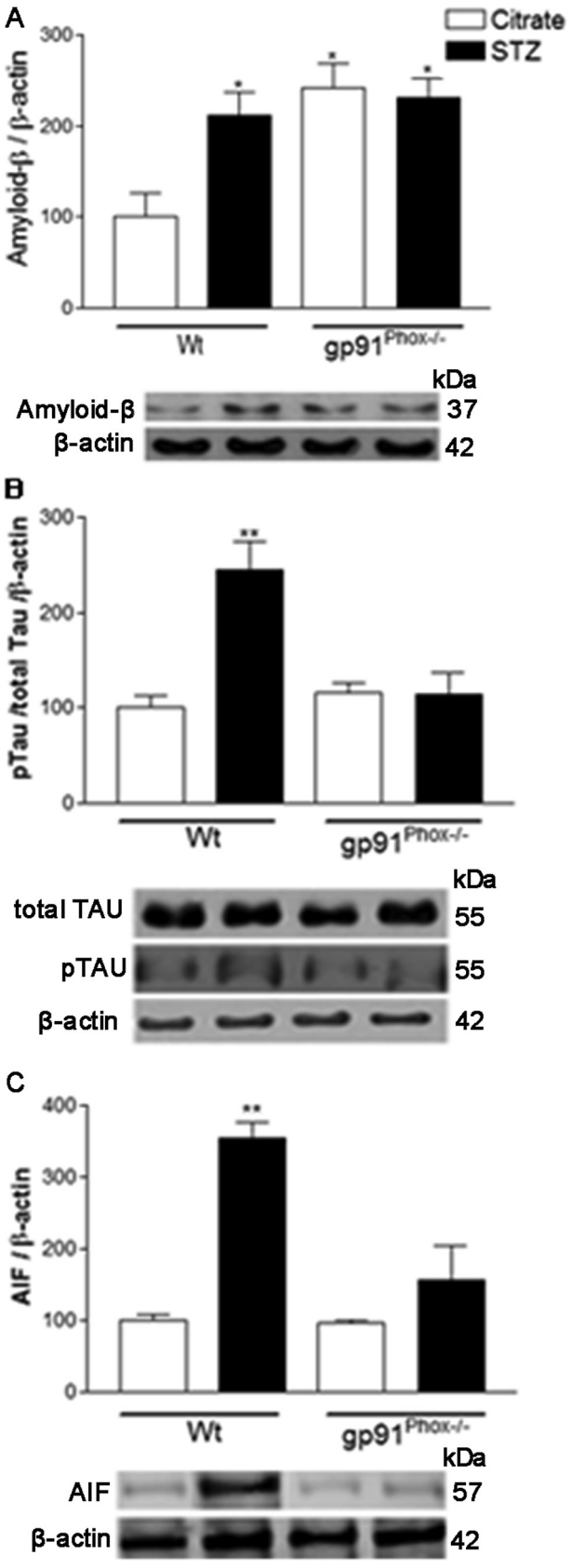

Fig. 4. Effect of STZ on Aβ expression (A), Tau phosphorylation (B) and AIF (C) in the hippocampus. The graphs represent mean ratio of Aβ, Tau phosphorylation and AIF densitometric data in relation to β-actin (n = 3–5). $^{*}P < 0.05$ *vs* Wt control group, $^{**}P < 0.01$ *vs* Wt control group (Tukey's test). STZ = streptozotocin, AIF = apoptosis-inducing factor.

damage, neuronal death and inflammation in the hippocampus of the STZ-induced AD-like mouse model. Our findings demonstrate that (1) Nox2 mRNA expression is upregulated following the STZ treatment; (2) Nox2 deletion protects mice against cognitive impairment and prevents Tau phosphorylation, oxidative damage, neuronal death and neuroinflammation induced by STZ; (3) The production of the antiinflammatory cytokine IL-10 was found significantly increased following Nox2 deletion.

Oxidative stress plays an important role in the pathogenesis of AD (Zhou et al., 2008). The hippocampus of AD patients has been shown to present increased 4-HNE reactivity in amyloid deposits, suggesting ROS mediated lipid peroxidation in amyloid deposits (Ando et al., 1998). Moreover, the levels of 3-NT, a marker of oxidative damage induced by tyrosine nitration were found increased in neurofibrillary tangles (Good et al., 1996). Corroborating our results in Wt mice, it has been previously demonstrated that the icv injection of STZ induces increased expression of HNE (Ishrat et al., 2009; Khan et al., 2012; Zhou et al., 2013) and 3-NT (Shoham et al., 2007) in the hippocampus of rats. Although oxidative stress has been shown to play a role in STZ-induced AD (Javed et al., 2011, 2012), the role of Nox2-derived ROS is still unclear. We found that Nox2 deletion prevented the oxidative damage to proteins and lipids induced by STZ.

Mild cognitive impairment and early AD are characterized by loss of synapses and connectivity, which occurs in parallel with NADPH-oxidase upregulation (mainly Nox2) in frontal and temporal cortex (Ansari and Scheff, 2011). Our data demonstrate that Nox2 gene expression was increased in the hippocampus following STZ-treatment, suggesting that Nox2 may play a role in STZ-induced AD.

Several studies have described that icv injections of STZ induce memory loss in mice (Sharma et al., 2008; Pinton et al., 2010; Tota et al., 2010), which has been associated with oxidative stress (Song et al., 2014). As expected, the STZ treatment induced a significant impairment in both short- and long-term object recognition memory in Wt mice. However, Nox2 deletion significantly protected mice against the short- and long-term memory deficit induced by STZ. This result suggested that Nox2 plays an essential role in the cognitive impairment induced by STZ. In agreement with our data, mice overexpressing the amyloid precursor protein Tg2576 and lacking Nox2 presented improved cognitive performance as revealed by the Morris water maze test, when compared to control littermates (Park et al., 2008).

There is a strong link between Aβ expression, neurodegeneration, ROS generation and AD development. The excessive production of Aβ peptide or its reduced clearance has been reported to induce amyloid aggregation, contributing to the generation of neurofibrillary tangles and subsequent neuronal degeneration in AD (Kar et al., 2004). In addition, $A\beta_{42}$ induced Nox-dependent ROS generation in primary astrocytes (Zhu et al., 2006). Corroborating our previous observations (Ravelli et al., 2017), icv injections of STZ

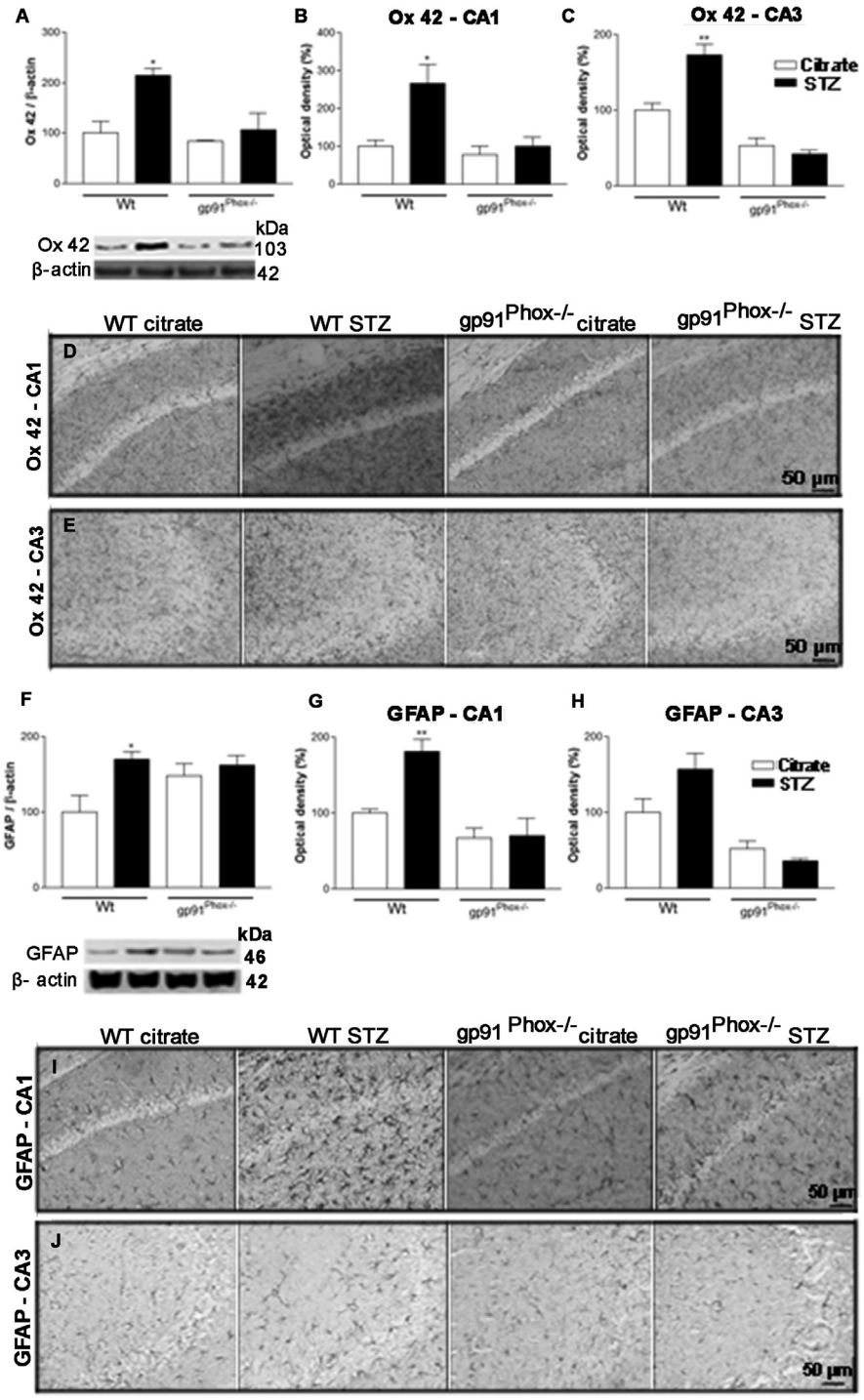

Fig. 5. Effects of STZ on OX42 and GFAP expression in the hippocampus of Wt and gp91$^{phox-/-}$ mice. (A) Western blots analysis of the Ox42 protein levels. The graphs represent mean ratio of Ox42 densitometric data in relation to β-actin. (B) Mean optical density of OX42 immunostaining in CA1 area. (C) Mean optical density of OX42 immunostaining in CA3 area. (D) Representative digital images of OX42-like immunoreactivity in CA1 area. (E) Representative digital images of OX42-like immunoreactivity in CA3 area. (F) Western blots analysis of the GFAP protein levels. The graphs represent mean ratio of GFAP densitometric data in relation to β-actin. (G) Mean optical density of GFAP immunostaining in CA1 area. (H) Mean optical density of GFAP immunostaining in CA3 area. (I) Representative digital images of GFAP-like immunoreactivity in CA1 area. (J) Representative digital images of GFAP-like immunoreactivity in CA3 area. (n = 3–5) $^{*}P < 0.05$ *vs* Wt control group and $^{**}P < 0.01$ *vs* Wt control group (Tukey's test). STZ = streptozotocin.

increase Aβ expression in the hippocampus of Wt mice. However, Nox2 deletion prevented the increased Aβ expression induced by STZ. Although Aβ expression was not found upregulated in gp91$^{phox-/-}$ mice following STZ, the baseline expression of this protein was found significantly increased in the hippocampus following Nox2 deletion. Our data suggest that: 1) Aβ expression might not be associated with the improved short- and long-term memory deficit observed in gp91$^{phox-/-}$ mice; and 2) Nox2 has a role in Aβ processing and accumulation induced by STZ. Similarly, the behavioral improvement observed in Tg2576-lacking Nox2 mice was not correlated with reductions in brain Aβ protein levels. Consistent with our results, the authors suggest that amyloid deposition can be dissociated from the behavioral deficits (Park et al., 2008).

Natural Aβ dimers isolated from the AD brain induce AD-type Tau phosphorylation and neuritic dystrophy in rat primary hippocampal neurons (Jin et al., 2011). In AD, neurofilaments found in neurofibrillary tangles, as well as Tau protein, are extensively phosphorylated (Liu et al., 2011a,b). In our study we observed that the STZ treatment was able to increase Tau phosphorylation in Wt animals, but not in gp91$^{phox-/-}$ mice. This finding suggests that Nox2-derived ROS is involved in Tau phosphorylation induced by STZ.

AIF is a mitochondrial intermembrane flavoprotein that translocates to the nucleus, and activates nuclear endonucleases, inducing chromatin condensation and DNA degradation, resulting in cellular death. Moreover, it induces the release of mitochondria-derived apoptogenic proteins, such as cytochrome *c* and caspase-9 (Susin et al., 1999). AD patients exhibit a significant increase in neuronal AIF immunoreactivity in the hippocampus (Yu et al., 2010; Lee et al., 2012), amygdala and cholinergic neurons of the basal forebrain, suggesting that AIF-induced apoptosis may contribute to neuronal death in AD (Lee et al., 2012). We found

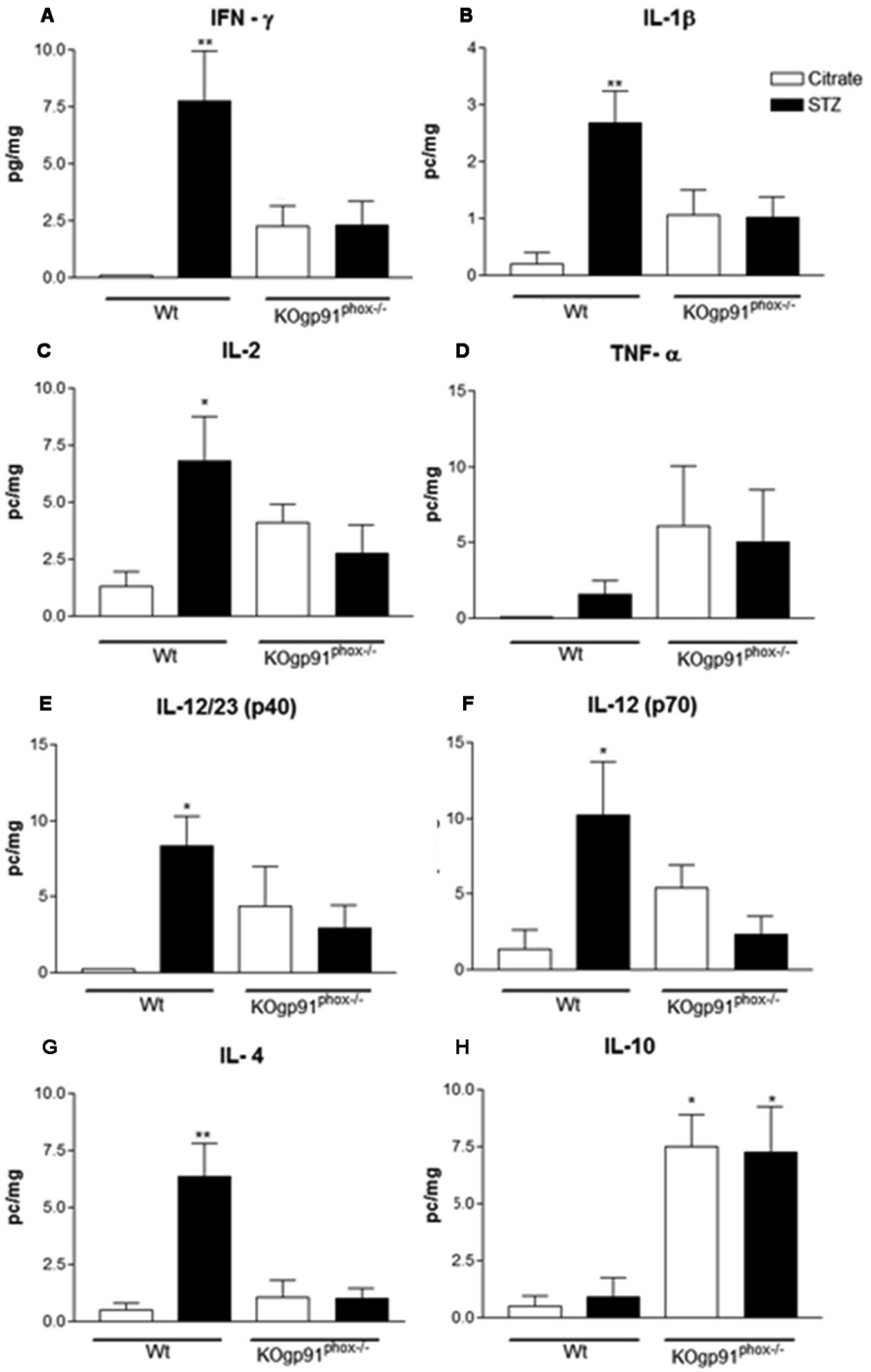

Fig. 6. Effect of STZ on Hippocampal cytokine concentration in Wt and gp91$^{phox-/-}$ mice. Concentration of pro-inflammatory (IL-1β, IL-2, IFN-γ, TNF-α, IL-12/23 [p40] and IL-12 [p70]) and anti-inflammatory cytokines (IL-4 and IL-10) in the hippocampus following STZ injection. All concentrations were expressed in pg/mg. (n = 5–8) $^{*}P < 0.05$ *vs* Wt control group and $^{**}P < 0.01$ *vs* Wt control group (Tukey's test). STZ = streptozotocin.

that expression of AIF was increased in STZ-treated Wt mice. Importantly, Nox2 deletion prevented increased hippocampal AIF expression induced by STZ. The influence of Nox2 in apoptosis has been previously demonstrated in an ischemic brain injury study. In that study, Nox2 activation was demonstrated to release of apoptogenic factors (AIF and cytochrome c) from mitochondria in brain tissue (Kim et al., 2012).

In AD brains, activated astrocytes and microglia are found in senile plaques and release cytokines, interleukins, ROS and other potentially cytotoxic molecules, thus exacerbating the neuroinflammatory response (Heneka et al., 2015). It has been previously described that STZ injection induces both microglia and astrocyte activation in the hippocampus of rats (Shoham et al., 2007). In this study immunoblotting data revealed increased expression of microglia and astrocyte markers in the hippocampus after icv STZ injection in Wt mice. Immunohistochemical detection of OX42-positive cells indicated marked microglial activation in both CA1 and CA3 areas. Our immunostaining assays also revealed increased expression of astrocyte markers in CA1 area after STZ injection. Our data suggest that gp91$^{phox-/-}$ mice are protected against glial activation induced by STZ. Similar results were observed in different neurodegenerative conditions, such as Parkinson's disease (Hernandes et al., 2013) and in sepsis-induced encephalopathy (Hernandes et al., 2014).

We further investigated the impact of Nox2 in mediating inflammatory responses in the hippocampal STZ-induced neurodegeneration. Nox2 deletion prevented the release of the proinflammatory cytokines IFN-γ, IL-1β, IL-2, IL-12/23 in the hippocampus following STZ treatment. Interferon is a potent activator of glial cells in the central nervous system. Many IFNγ responsive genes are upregulated in AD (Chakrabarty et al., 2010). IFNγ-induced priming of microglia stimulates upregulation of Nox2 (Spencer et al., 2016). This cytokine promotes the release of proinflammatory cytokines such as tumor necrosis factor-α (TNF-α) and IL-1β (Mangano et al., 2012) (another proinflammatory cytokine upregulated after STZ injection). Corroborating with our data, the expression of IL-1β was also found increased after icv STZ injection in Wt rats (Chu et al., 2014). Oligomeric Aβ induces the secretion of this cytokine in LPS-primed microglia, which is partially dependent on Nox2-derived ROS production (Parajuli et al., 2013).

In AD the expression of IL-12 and IL-23 is increased in microglia and the expression of the respective receptors

by astrocytes is also increased (Heppner et al., 2015). Both of these cytokines are produced by microglia in mouse models of Alzheimer's disease and its inhibition reduces AD-like pathology (Heneka et al., 2015). The levels of IL-2 and its receptor immunoreactivity are also significantly increased in AD. This cytokine appears to decrease hippocampal acetylcholine levels and to reduce neuronal survival (Araujo and Lapchak, 1994).

IL-10, another potent anti-inflammatory cytokine, has been reported to reduce inflammation in AD (Lee et al., 2009). IL-10 limits inflammation by suppressing proinflammatory cytokines production (Swardfager et al., 2010), suppressing cytokine receptor expression and inhibiting markers of activation (Lee et al., 2009). Endogenous IL-10 expressed in microglia prevented LPS-induced neurodegeneration in rat cerebral cortex *in vivo* and the inhibition of IL-10 upregulated both LPS-induced Nox activation and the expression of pro-inflammatory mediators (Park et al., 2007). In our study, STZ treatment was not able to stimulate IL-10 synthesis in either Wt or gp91$^{phox-/-}$ mice. However, Nox2 deletion had a profound positive effect on the IL-10 baseline production, suggesting that IL-10 contributes to the neuroprotection mechanism against STZ-induced neurodegeneration. Future studies are necessary to uncover exactly how Nox2 deletion modulates IL-10 release and leads to neuroprotection in the STZ-induced AD-like state.

CONCLUSIONS

In summary, our data suggest that the Nox2-dependent oxidative stress generation contributes to the STZ-induced AD-like state via multiple mechanisms. Nox2 deletion prevented Tau phosphorylation, Aβ expression and decreased neuroinflammation in hippocampi after STZ treatment. Moreover, the baseline IL-10 levels were found profoundly increased following Nox2 deletion, suggesting that this is one of the potential mechanisms by which gp91$^{phox-/-}$ mice are protected against STZ-induced AD-like state. Altogether, those different mechanisms may contribute to the protection observed in those mice.

ETHICAL APPROVAL

All procedures performed in studies involving animals were in accordance with the ethical standards of the institution at which the studies were conducted.

This article does not contain any studies with human participants performed by any of the authors.

Acknowledgments—Work supported by FAPESP (Fundação de Amparo à Pesquisa do Estado de São Paulo), University of São Paulo-NAPNA (Núcleo de Apoio à Pesquisa em Neurociência Aplicada) and CNPq (Conselho Nacional de Desenvolvimento Científico e Tecnológico). K.G.R. (2012/01444-7), B. R.A. (2013/16364-1) were the recipients of fellowships from FAPESP . M.S.H was recipient of. FAPESP 24660-0 and AHA 17SDG33410777 Grants. Thanks are due to Adilson S. Alves for technical assistance.

REFERENCES

Ando Y, Brännström T, Uchida K, Nyhlin N, Näsman B, Suhr O, Yamashita T, Olsson T, El Salhy M, Uchino M, Ando M (1998) Histochemical detection of 4-hydroxynonenal protein in Alzheimer amyloid. J Neurol Sci 156:172–176.

Ansari MA, Scheff SW (2011) NADPH-oxidase activation and cognition in Alzheimer disease progression. Free Radic Biol Med 51:171–178.

Araujo DM, Lapchak PA (1994) Induction of immune system mediators in the hippocampal formation in Alzheimer's and Parkinson's diseases: selective effects on specific interleukins and interleukin receptors. Neuroscience 61:745–754.

Bird TD (2008) Genetic aspects of Alzheimer disease. Genet Med 10:231–239.

Block ML (2008) NADPH oxidase as a therapeutic target in Alzheimer's disease. BMC Neurosci 9(Suppl 2):S8.

Bomfim TR, Forny-Germano L, Sathler LB, Brito-Moreira J, Houzel JC, Decker H, Silverman MA, Kazi H, Melo HM, McClean PL, Holscher C, Arnold SE, Talbot K, Klein WL, Munoz DP, Ferreira ST, De Felice FG (2012) An anti-diabetes agent protects the mouse brain from defective insulin signaling caused by Alzheimer's disease- associated Abeta oligomers. J Clin Invest 122:1339–1353.

Bonda DJ, Wang X, Perry G, Nunomura A, Tabaton M, Zhu X, Smith MA (2010) Oxidative stress in Alzheimer disease: a possibility for prevention. Neuropharmacology 59:290–294.

Bruce-Keller AJ, Gupta S, Parrino TE, Knight AG, Ebenezer PJ, Weidner AM, LeVine 3rd H, Keller JN, Markesbery WR (2010) NOX activity is increased in mild cognitive impairment. Antioxid Redox Signal 12:1371–1382.

Chakrabarty P, Ceballos-Diaz C, Beccard A, Janus C, Dickson D, Golde TE, Das P (2010) IFN-gamma promotes complement expression and attenuates amyloid plaque deposition in amyloid beta precursor protein transgenic mice. J Immunol 184:5333–5343.

Chen Y, Liang Z, Blanchard J, Dai CL, Sun S, Lee MH, Grundke-Iqbal I, Iqbal K, Liu F, Gong CX (2013) A non-transgenic mouse model (icv-STZ mouse) of Alzheimer's disease: Similarities to and differences from the transgenic model (3xTg-AD mouse). Mol Neurobiol 47:711–725.

Chu S, Gu J, Feng L, Liu J, Zhang M, Jia X, Liu M, Yao D (2014) Ginsenoside Rg5 improves cognitive dysfunction and beta-amyloid deposition in STZ-induced memory impaired rats via attenuating neuroinflammatory responses. Int Immunopharmacol 19:317–326.

Dumont M, Stack C, Elipenhali C, Calingasan NY, Wille E, Beal MF (2011) Apocynin administration does not improve behavioral and neuropathological deficits in a transgenic mouse model of Alzheimer's disease. Neurosci Lett 492:150–154.

Dussault AA, Pouliot M (2006) Rapid and simple comparison of messenger RNA levels using real-time PCR. Biol Proced Online 8:1–10.

Fox C, Dingman A, Derugin N, Wendland MF, Manabat C, Ji S, Ferriero DM, Vexler ZS (2005) Minocycline confers early but transient protection in the immature brain following focal cerebral ischemia-reperfusion. J Cereb Blood Flow Metab 25:1138–1149.

Good PF, Werner P, Hsu A, Olanow CW, Perl PD (1996) Evidence of neuronal oxidative damage in Alzheimer's disease. Am J Pathol 149:21–28.

Grunblatt E, Hoyer S, Riederer P (2004) Gene expression profile in streptozotocin rat model for sporadic Alzheimer's disease. J Neural Transm 111:367–386.

Hardy J, Allsop D (1991) Amyloid deposition as the central event in the aetiology of Alzheimer's disease. Trends Pharmacol Sci 12:383–388.

Heneka MT et al (2015) Neuroinflammation in Alzheimer's disease. Lancet Neurol 14:388–405.

Heppner FL, Ransohoff RM, Becher B (2015) Immune attack: the role of inflammation in Alzheimer disease. Nat Rev Neurosci 16:358–372.

Hernandes MS, Britto LR (2012) NADPH oxidase and neurodegeneration. Curr Neuropharmacol 10:321–327.
Hernandes MS, Cafe-Mendes CC, Britto LR (2013) NADPH oxidase and the degeneration of dopaminergic neurons in parkinsonian mice. Oxid Med Cell Longev 2013:157857.
Hernandes MS, D'Avila JC, Trevelin SC, Reis PA, Kinjo ER, Lopes LR, Castro-Faria-Neto HC, Cunha FQ, Britto LR, Bozza FA (2014) The role of Nox2-derived ROS in the development of cognitive impairment after sepsis. J Neuroinflammation 11:36.
Ishrat T, Hoda MN, Khan MB, Yousuf S, Ahmad M, Khan MM, Ahmad A, Islam F (2009) Amelioration of cognitive deficits and neurodegeneration by curcumin in rat model of sporadic dementia of Alzheimer's type (SDAT). Eur Neuropsychopharmacol 19:636–647.
Javed H, Khan M, Khan A, Vaibhav K, Ahmad A, Khuwaja G, Ahmed ME, Raza SS, Ashafaq M, Tabassum R, Siddiqui MS, El-Agnaf OM, Safhi MM, Islam F (2011) S-allyl cysteine attenuates oxidative stress associated cognitive impairment and neurodegeneration in mouse model of streptozotocin-induced experimental dementia of Alzheimer's type. Brain Res 10:133–142.
Javed H, Khan M, Ahmad A, Vaibhav K, Ahmad ME, Khan A, Ashafaq M, Islam F, Siddiqui MS, Safhi MM (2012) Rutin prevents cognitive impairments by ameliorating oxidative stress and neuroinflammation in rat model of sporadic dementia of Alzheimer type. Neuroscience 210:340–352.
Jin M, Shepardson N, Yang T, Chen G, Walsh D, Selkoe DJ (2011) Soluble amyloid beta-protein dimers isolated from Alzheimer cortex directly induce Tau hyperphosphorylation and neuritic degeneration. Proc Natl Acad Sci U S A 108:5819–5824.
Kar S, Slowikowski SP, Westaway D, Mount HT (2004) Interactions between beta-amyloid and central cholinergic neurons: implications for Alzheimer's disease. J Psychiatry Neurosci 29:427–441.
Khan MB, Khan MM, Khan A, Ahmed ME, Ishrat T, Tabassum R, Vaibhav K, Ahmad A, Islam F (2012) Naringenin ameliorates Alzheimer's disease (AD)-type neurodegeneration with cognitive impairment (AD-TNDCI) caused by the intracerebroventricular-streptozotocin in rat model. Neurochem Int 61:1081–1093.
Kim GS, Jung JE, Narasimhan P, Sakata H, Yoshioka H, Song YS, Okami N, Chan PH (2012) Release of mitochondrial apoptogenic factors and cell death are mediated by CK2 and NADPH oxidase. J Cereb Blood Flow Metab 32:720–730.
Knezovic A, Osmanovic-Barilar J, Curlin M, Hof PR, Simic G, Riederer P, Salkovic-Petrisic M (2015) Staging of cognitive deficits and neuropathological and ultrastructural changes in streptozotocin-induced rat model of Alzheimer's disease. J Neural Transm 122:577–592.
Lee KS, Chung JH, Choi TK, Suh SY, Oh BH, Hong CH (2009) Peripheral cytokines and chemokines in Alzheimer's disease. Dement Geriatr Cogn Disord 28:281–287.
Lee JH, Cheon YH, Woo RS, Song DY, Moon C, Baik TK (2012) Evidence of early involvement of apoptosis inducing factor-induced neuronal death in Alzheimer brain. Anat Cell Biol 45:26–37.
Liu Q, Xie F, Alvarado-Diaz A, Smith MA, Moreira PI, Zhu X, Perry G (2011a) Neurofilamentopathy in neurodegenerative diseases. Open Neurol J 5:58–62.
Liu Y, Liu F, Grundke-Iqbal I, Iqbal K, Gong CX (2011b) Deficient brain insulin signalling pathway in Alzheimer's disease and diabetes. J Pathol 225:54–62.
Mangano EN, Litteljohn D, So R, Nelson E, Peters S, Bethune C, Bobyn J, Hayley S (2012) Interferon-gamma plays a role in paraquat-induced neurodegeneration involving oxidative and proinflammatory pathways. Neurobiol Aging 33:1411–1426.
Moloney AM, Griffin RJ, Timmons S, O'Connor R, Ravid R, O'Neill C (2010) Defects in IGF-1 receptor, insulin receptor and IRS-1/2 in Alzheimer's disease indicate possible resistance to IGF-1 and insulin signalling. Neurobiol Aging 31:224–243.
Moncunill G, Aponte JJ, Nhabomba AJ, Dobaño C (2013) Performance of multiplex commercial kits to quantify cytokine and chemokine responses in culture supernatants from Plasmodium falciparum stimulations. PLoS ONE 8:52587.
Parajuli B, Sonobe Y, Horiuchi H, Takeuchi H, Mizuno T, Suzumura A (2013) Oligomeric amyloid beta induces IL-1beta processing via production of ROS: implication in Alzheimer's disease. Cell Death Dis 4:e975.
Park L, Anrather J, Zhou P, Frys K, Pitstick R, Younkin S, Carlson GA, Iadecola C (2005) NADPH-oxidase-derived reactive oxygen species mediate the cerebrovascular dysfunction induced by the amyloid beta peptide. J Neurosci 25:1769–1777.
Park KW, Lee HG, Jin BK, Lee YB (2007) Interleukin-10 endogenously expressed in microglia prevents lipopolysaccharide-induced neurodegeneration in the rat cerebral cortex in vivo. Exp Mol Med 39:812–819.
Park L et al (2008) Nox2-derived radicals contribute to neurovascular and behavioral dysfunction in mice overexpressing the amyloid precursor protein. Proc Natl Acad Sci 105:1347–1352.
Park KW, Baik HH, Jin BK (2009) IL-13-induced oxidative stress via microglial NADPH oxidase contributes to death of hippocampal neurons in vivo. J Immunol 183:4666–4674.
Pinton S, da Rocha JT, Zeni G, Nogueira CW (2010) Organoselenium improves memory decline in mice: involvement of acetylcholinesterase activity. Neurosci Lett 472:56–60.
Ravelli KG, Rosário BA, Camarini R, Hernandes MS, Britto LR (2017) Intracerebroventricular streptozotocin as a model of Alzheimer's disease: neurochemical and behavioral characterization in mice. Neurotox Res 31:327–333.
Selkoe DJ (2001) Alzheimer's disease: genes, proteins, and therapy. Physiol Rev 81:741–766.
Serrano-Pozo A, Frosch MP, Masliah E, Hyman BT (2011) Neuropathological alterations in Alzheimer disease. Cold Spring Harb Perspect Med 1:a006189.
Sharma B, Singh N, Singh M, Jaggi AS (2008) Exploitation of HIV protease inhibitor Indinavir as a memory restorative agent in experimental dementia. Pharmacol Biochem Behav 89:535–545.
Shoham S, Bejar C, Kovalev E, Schorer-Apelbaum D, Weinstock M (2007) Ladostigil prevents gliosis, oxidative-nitrative stress and memory deficits induced by intracerebroventricular injection of streptozotocin in rats. Neuropharmacology 52:836–843.
Song J et al (2014) Agmatine improves cognitive dysfunction and prevents cell death in a streptozotocin-induced Alzheimer rat model. Yonsei Med J 55:689–699.
Spencer NG, Schilling T, Miralles F, Eder C (2016) Mechanisms Underlying Interferon-gamma-Induced Priming of Microglial Reactive Oxygen Species Production. PLoS ONE 11:e0162497.
Spires TL, Hyman BT (2005) Transgenic models of Alzheimer's disease: learning from animals. NeuroRx 2:423–437.
Susin SA, Lorenzo HK, Zamzami N, Marzo I, Snow BE, Brothers GM, Mangion J, Jacotot E, Costantini P, Loeffler M, Larochette N, Goodlett DR, Aebersold R, Siderovski DP, Penninger JM, Kroemer G (1999) Molecular characterization of mitochondrial apoptosis-inducing factor. Nature 397:441–446.
Swardfager W, Lanctôt K, Rothenburg L, Wong A, Cappell J, Herrmann N (2010) A meta-analysis of cytokines in Alzheimer's disease. Biol Psychiatry 68:930–941.
Szkudelski T (2001) The mechanism of alloxan and streptozotocin action in B cells of the rat pancreas. Physiol Res 50:537–546.
Talbot K, Wang HY, Kazi H, Han LY, Bakshi KP, Stucky A, Fuino RL, Kawaguchi KR, Samoyedny AJ, Wilson RS, Arvanitakis Z, Schneider JA, Wolf BA, Bennett DA, Trojanowski JQ, Arnold SE (2012) Demonstrated brain insulin resistance in Alzheimer's disease patients is associated with IGF-1 resistance, IRS-1 dysregulation, and cognitive decline. J Clin Invest 122:1316–1338.
Tota S, Awasthi H, Kamat PK, Nath C, Hanif K (2010) Protective effect of quercetin against intracerebral streptozotocin induced reduction in cerebral blood flow and impairment of memory in mice. Behav Brain Res 209:73–79.

Wilkinson BL et al (2012) Ibuprofen attenuates oxidative damage through NOX2 inhibition in Alzheimer's disease. Neurobiol Aging 33:197. p. 197 e21-32.

Yarchoan M, Toledo JB, Lee EB, Arvanitakis Z, Kazi H, Han LY, Louneva N, Lee VM, Kim SF, Trojanowski JQ, Arnold SE (2014) Abnormal serine phosphorylation of insulin receptor substrate 1 is associated with tau pathology in Alzheimer's disease and tauopathies. Acta Neuropathol 128:679–689.

Yu W, Mechawar N, Krantic S, Quirion R (2010) Evidence for the involvement of apoptosis-inducing factor-mediated caspase-independent neuronal death in Alzheimer disease. Am J Pathol 176:2209–2218.

Zhou J, Zhang S, Zhao X, Wei T (2008) Melatonin impairs NADPH oxidase assembly and decreases superoxide anion production in microglia exposed to amyloid-beta1-42. J Pineal Res 45:157–165.

Zhou S, Yu G, Chi L, Zhu J, Zhang W, Zhang Y, Zhang L (2013) Neuroprotective effects of edaravone on cognitive deficit, oxidative stress and tau hyperphosphorylation induced by intracerebroventricular streptozotocin in rats. Neurotoxicology 38:136–145.

Zhu D, Lai Y, Shelat PB, Hu C, Sun GY, Lee JC (2006) Phospholipases A2 mediate amyloid-beta peptide-induced mitochondrial dysfunction. J Neurosci 26:11111–11119.

(Received 14 March 2017, Accepted 26 June 2017)
(Available online 4 July 2017)